

# Natural Plant Materials as Dielectric Layer for Highly Sensitive Flexible Electronic Skin

Yongbiao Wan, Zhiguang Qiu, Jun Huang, Jingyi Yang, Qi Wang, Peng Lu, Junlong Yang, Jianming Zhang, Siya Huang, Zhigang Wu, and Chuan Fei Guo\*

Nature has long offered human beings with useful materials. Herein, plant materials including flowers and leaves have been directly used as the dielectric material in flexible capacitive electronic skin (e-skin), which simply consists of a dried flower petal or leaf sandwiched by two flexible electrodes. The plant material is a 3D cell wall network which plays like a compressible metamaterial that elastically collapses upon pressing plus some specific surface structures, and thus the device can sensitively respond to pressure. The device works over a broad-pressure range from 0.6 Pa to 115 kPa with a maximum sensitivity of  $1.54 \text{ kPa}^{-1}$ , and shows high stability over 5000 cyclic pressings or bends. The natural-material-based e-skin has been applied in touch sensing, motion monitoring, gas flow detection, and the spatial distribution of pressure. As the foam-like structure is ubiquitous in plants, a general strategy for a green, cost-effective, and scalable approach to make flexible e-skins is offered here.


Remarkable advances have been achieved in the field of flexible electronics in the last two decades. Electronic skins (e-skins) are important devices to human-centric electronics, human-machine interaction, and soft robotics by enabling machines with tactile senses.<sup>[1–6]</sup> An ideal e-skin is expected to be highly sensitive, flexible, light weight, inexpensive, environmentally friendly, and easy to fabricate. The existing e-skins

Y. Wan, Z. Qiu, J. Huang, J. Yang, Q. Wang, P. Lu, Dr. J. Yang,  
Prof. J. Zhang, Prof. S. Huang, Prof. Z. Wu, Prof. C. F. Guo  
Department of Materials Science and Engineering  
Southern University of Science and Technology  
Shenzhen 518055, China  
E-mail: guocf@sustc.edu.cn

Y. Wan, J. Huang, P. Lu  
School of Materials Science and Engineering  
Harbin Institute of Technology  
Harbin 150001, China

Prof. J. Zhang, Prof. S. Huang  
Academy for Advanced Interdisciplinary Studies  
Southern University of Science and Technology  
Shenzhen 518055, China

Prof. Z. Wu  
State Key Laboratory of Digital Manufacturing Equipment and  
Technology  
Huazhong University of Science and Technology  
Wuhan 430074, China

 The ORCID identification number(s) for the author(s) of this article can be found under <https://doi.org/10.1002/smll.201801657>.

DOI: 10.1002/smll.201801657

are typically based on four mechanisms and corresponding devices are piezoresistive,<sup>[7,8]</sup> capacitive,<sup>[9,10]</sup> piezoelectric,<sup>[11,12]</sup> and triboelectric types,<sup>[13,14]</sup> and capacitive type e-skins are extensively investigated because capacitive sensors often have a simple structure, fast response time, high sensitivity and stability, and present higher precision than other electrical sensors.<sup>[2,15]</sup>

A typical structure of the capacitive type e-skin consists of a polymeric dielectric layer (typically elastomer) sandwiched by two flexible electrodes.<sup>[15,16]</sup> Dielectric materials with microstructures such as pores,<sup>[17–19]</sup> pyramids,<sup>[10,20–22]</sup> microspheres,<sup>[23,24]</sup> have been used to improve the sensitivity because these microstructures are more easily to be compressed than flat films. Many such microstructures are fabricated by using lithographic

methods,<sup>[10,20–22]</sup> in which expensive facilities and hazardous chemicals are often used. Although some recent works have successfully cut the fabrication cost by using unconventional methods including surface wrinkling,<sup>[25]</sup> templating with a rough surface,<sup>[26]</sup> or electrospinning of nanofibers,<sup>[27]</sup> the material systems have not yet been changed, and the man-made polymeric dielectric materials are typically not degradable or sustainable. In addition, e-skins with surface microstructures, such as micropylamids,<sup>[22]</sup> exhibit nonlinear signals to the pressure and the signal gets saturated at high pressures.

Herein, we reported a simple method that directly applies plant materials including leaves and petals as the dielectric layer in capacitive type e-skins. The natural materials used in this study include rose petals, rose leaves, and *Acacia Mill* leaves. We treated the natural materials by critical point drying, which removes water from the materials to significantly improve the stability while well keeping the surface morphology and inner structures. The device using dried rose petal exhibits a high sensitivity of  $1.54 \text{ kPa}^{-1}$  in a low pressure regime ( $<1 \text{ kPa}$ ), and exceptional stability over 5000 cyclic loading/unloading or 5000 cyclic bends at a bending radius of 3 mm. In existing works, surface microstructures have often been used to improve the sensitivity whereas the material is intrinsically incompressible;<sup>[10,18,19]</sup> here the dried petal or leaf is a foam-like hollow structure (which is ubiquitous in plants) of a 3D network of cell walls, and can be regarded as a highly compressible metamaterial. In addition, the surface microstructures of plant materials also contribute to the compressibility. The e-skins with natural

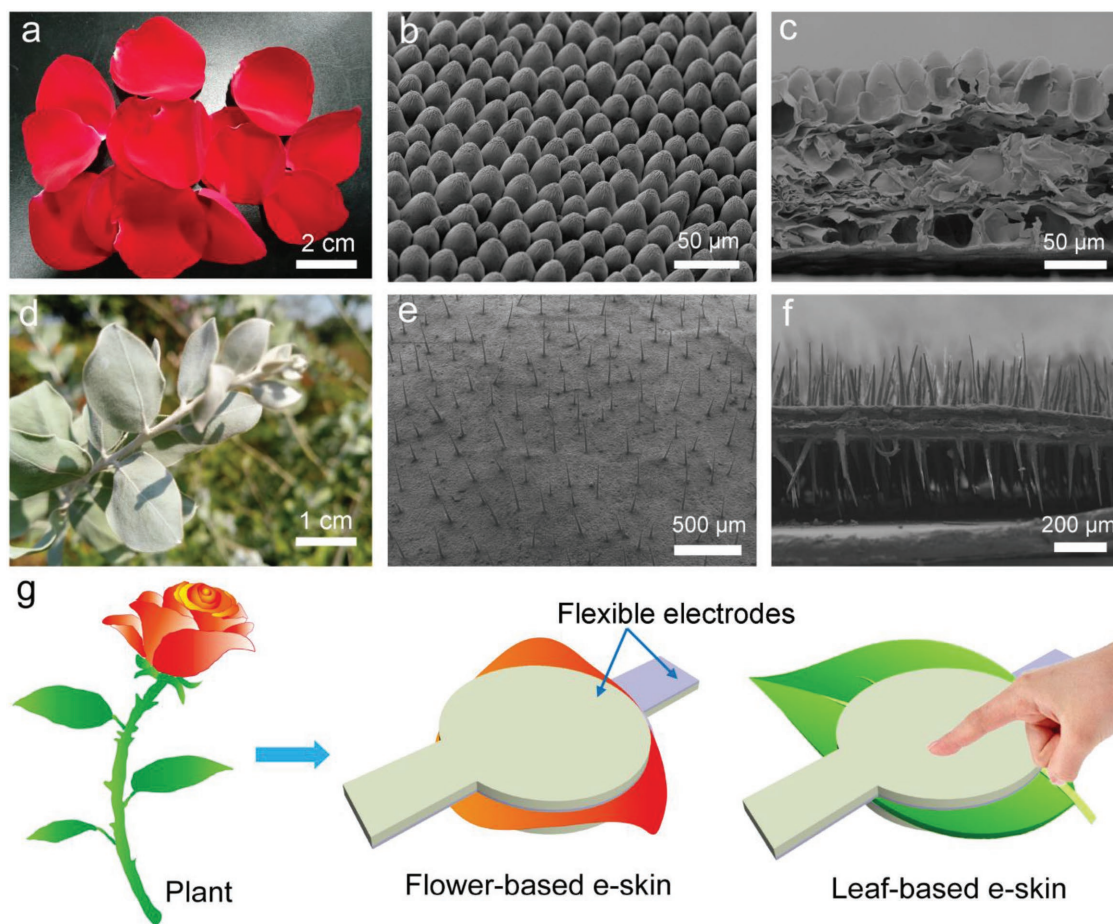


**Figure 1.** Natural materials and device structure. a) Photograph of red rose petals. b) A 45° tilted view SEM image of the rose petal dried by critical point drying. c) Cross-sectional SEM image of the rose petal. d) Photograph of *Acacia Mill* leaves. e) Surface morphology of the *Acacia Mill* leaf, showing needle-like structures on the surface. f) Cross-sectional SEM image of the *Acacia Mill* leaf. g) Schematic illustration of the e-skin consisting of two electrodes and the natural material as the dielectric layer in between.

materials as the dielectric layer has demonstrated possible applications in human motion monitoring, gesture recognition, and sensing of flows such as gas flow detection. We have also shown that the sensor array can accurately map the spatial distribution of applied pressures. The e-skin with natural materials may offer promising potentials in wearable electronics, artificial intelligence, soft robots, etc. Our strategy of directly using natural materials in e-skins is believed to put forward a cost-effective, environmentally friendly, and scalable approach to promote flexible electronics. We also predict that the compressible dielectrics of plant materials can be extended to many other natural materials that are not mentioned in this work.

We have studied three natural materials with different surface structures. The first material is rose petal. **Figure 1a** displays a photograph of red rose petals. Behind the romantic appearance, the rose petals hide some more beautiful morphology on their surfaces. Figure S1 (Supporting Information) shows the scanning electron microscopy (SEM) image of a naturally dried rose petal with shriveled microstructures. To maintain the surface features, fresh rose petals were treated by critical point drying, exhibiting uniform mastoid-like microstructures array, as shown in Figure 1b. The average diameter

and height of the mastoid microstructures are 23 and 40 μm, respectively. Further cross-sectional SEM image (Figure 1c) shows that the mastoid is a hollow structure with a thin shell, and the rose petal consists of a few layers of hollow structures from one surface to the other. In addition to the rose petals, rose leaves also have featured dense island-like microstructures with an average height of ≈10 μm and an average inter-island distance of ≈50 μm on the surface (see Figure S2, Supporting Information) and the whole leaf is hollow, either. The result is in accordance with the fact that mesophyll consists of a few layers of cells, and only the cell walls are left in a dried leaf. The third natural material is *Acacia Mill* leaves, which possess needle-like microstructures with a diameter of ≈25 μm and a height of ≈300 μm on both surfaces and the needles are kept after drying, as shown in Figure 1d–f.

The dried natural materials were directly used as the dielectric layer in capacitive type e-skins. A simple processing of the flexible capacitive e-skin is depicted in Figure 1g. The flexible e-skins consist of two electrodes placed face-to-face and the natural dielectric layer in between. The electrode was fabricated by spraying silver nanowires (AgNWs) onto a colorless polyimide (CPI) film (Figure S3, Supporting Information). The AgNWs

used in this work is dense and ultrathin (20 nm in diameter). Because of the small diameter and the high length to diameter aspect ratio of the AgNWs, together with the hydroxypropylmethyl cellulose (HPMC) coating which helps reduce the roughness and enhance the adhesion, the AgNW film is smooth and it exhibits a low sheet resistance of  $\approx 10 \Omega \cdot \text{sq}^{-1}$ .

The assembled device was subjected to a sensitivity measurement over the pressure range of 0.6 Pa–115 kPa covering the pressures generated by most daily activities.<sup>[3]</sup> The pressure applied on the device was gradually swept from 0.6 Pa to 115 kPa with a constant speed for each steps controlled by a force gauge. The sensitivity ( $S$ ) of capacitance to pressure is given by

$$S = \delta(\Delta C/C_0)/\delta P \quad (1)$$

where  $\Delta C$  is the variation of capacitance ( $C-C_0$ ),  $P$  presents applied pressure.<sup>[1]</sup> We first tested the sensing property of a device with a fresh rose petal substitutional to the dried petal or leaf. We also tested the frequency-dependent capacitances of the e-skins in unloading status. The fresh rose petal-based e-skin shows higher capacitances than naturally dried petal-based device, and the capacitance decreases with increasing tested frequency (Figure S4a, Supporting Information) due to the electrical double layer (EDL) contributed by the ionic liquid in fresh rose petal.<sup>[28,29]</sup> Such EDL effect of fresh rose petal-based e-skin remarks higher response than naturally dried petal (see Figure S4b, Supporting Information). The initial sensitivity is quite high. However, after two weeks, the maximum sensitivity of the device decreases from 2.1 to 0.78  $\text{kPa}^{-1}$ , as shown in **Figure 2a**, due to the drying of the fresh rose petal. The result indicates that the fresh petal although has a high sensitivity, its sensing stability is too low to fulfill with real applications. This is the reason that we choose dried petals or leaves instead of fresh ones. Figure 2b summarizes the capacitive-to-mechanical characteristics of the three e-skins based on dried rose petal, rose leaf, and *Acacia Mill* leaf with a fixed sensing surface area. Sensitivities of these e-skins are calculated as demonstrated in Figure 2c. As for rose-petal-based e-skin, three linear regions of the  $\Delta C$ - $P$  curve are observed. The maximum sensitivity value of 1.54  $\text{kPa}^{-1}$  was observed at the low pressure range (<1 kPa), which is higher than the cases using porous or pyramidal PDMS, and polystyrene microspheres as the dielectric layer.<sup>[10,17,23]</sup> As pressure increases, sensitivity decreases to 0.068  $\text{kPa}^{-1}$  in the region of 1–40 kPa and 0.014  $\text{kPa}^{-1}$  in the region of 40–115 kPa, with a trend that the sensitivity decreases with the increasing of pressure, similar to many other reported flexible e-skins.<sup>[30–32]</sup> However, the reported sensors typically have a saturated signal when the applied pressure is larger than 50 kPa. By contrast, our sensors still have a linear response to pressure at the high pressure range up to 115 kPa, which is larger than a standard atmospheric pressure. This result might be ascribed to the 3D network constructed by the stiff cell walls. It should be noted that the innate microstructures of natural plants cannot be precisely controlled, and thus variation of performances will exist in different devices. The deviation in performances might be acceptable in some applications. However, when high precision of the devices is required, all devices should be subjected to calibration before use.

The sensor with dried rose leaf exhibits an average sensitivity lower than the device with the rose petal as a result of lower porosity and relatively smooth surface. The device with *Acacia Mill* leaf, although showing a lower average sensitivity over the whole pressure range, has a higher sensitivity at the high pressure range and the higher sensitivity might be due to the special needle-like structures. The results indicate that natural materials with diverse surface structures can be offered as the dielectric layer for flexible e-skin.

In the sensing tests below, we only present the properties of the rose-petal-based e-skin. The response of the e-skin to ultralow pressure was characterized. As shown in Figure 2d, as the pressure was loaded from 0.6 to 3.0 Pa gradually, the capacitance shows a signal waveform very close to that of the input pressures. The result also indicates that the limit of detection (LOD) is at least lower than 0.6 Pa. In addition, different pressures of 0.1, 0.4, 10, and 110 kPa (Figure S5, Supporting Information) were successively applied onto the device to investigate the response towards dynamic forces, and the capacitance obviously increased with the increasing pressure as displayed in Figure 2e. The capacitance–pressure curve shows hysteresis and the loops of different cycles can well overlap (see Figure S6, Supporting Information). We have also tested the real-time response of the e-skin against the pressure of 0.2 kPa with different applied speed from 1 to 5  $\text{mm} \cdot \text{min}^{-1}$  (Figure 2f), and the e-skin produced an excellent match between the pressure and the response curve with stable, continuous, noise-free, and highly reproducible signals at various pressures (Figure S7, Supporting Information). Not only that, the sensor could accurately respond to successive pressure with the changing loading speed from 5 to 1  $\text{mm} \cdot \text{min}^{-1}$  (Figure 2g), indicating the potential in dynamic pressure detection.

Long-term stability is quite important to real applications. The sensor was loaded/unloaded at a repeated pressure of 150 Pa for 5000 times to investigate long-term stability (Figure 2h), and no drift was found throughout the 5000 cycles. The insets in Figure 2h show that at different stages of the test (from the beginning to the end) the signal well keeps the amplitude and waveform, confirming the high stability of the device. The stable performance is related to the stability in structure. Figure S8 (Supporting Information) shows a SEM image of the critical point dried rose petal after loading with a high pressure of 115 kPa, and no collapse or cracking was found in the surface. We have also tested the flexibility of the e-skin. A device was subjected to cyclic bends with a bending radius of 3 mm and showed no signal drift after 5000 cyclic bends (Figure 2i). The detailed inspection over ten bending cycles (Figure 2j) also indicates that the signal is generally stable, although tiny differences could be observed for different individual peaks. The bending test illustrates a fact: the natural-material-based e-skins have the potential to measure the strain caused by bending.

**Figure 3** illustrates the sensing mechanism of the natural material-based e-skin. The capacitance ( $C$ ) of the capacitive-type sensor is positively proportional to the effective area ( $A$ ) of the two electrodes, and the permittivity of the dielectric layer ( $\epsilon$ ), but inversely proportional with distance ( $d$ ) between the plate electrodes. That is



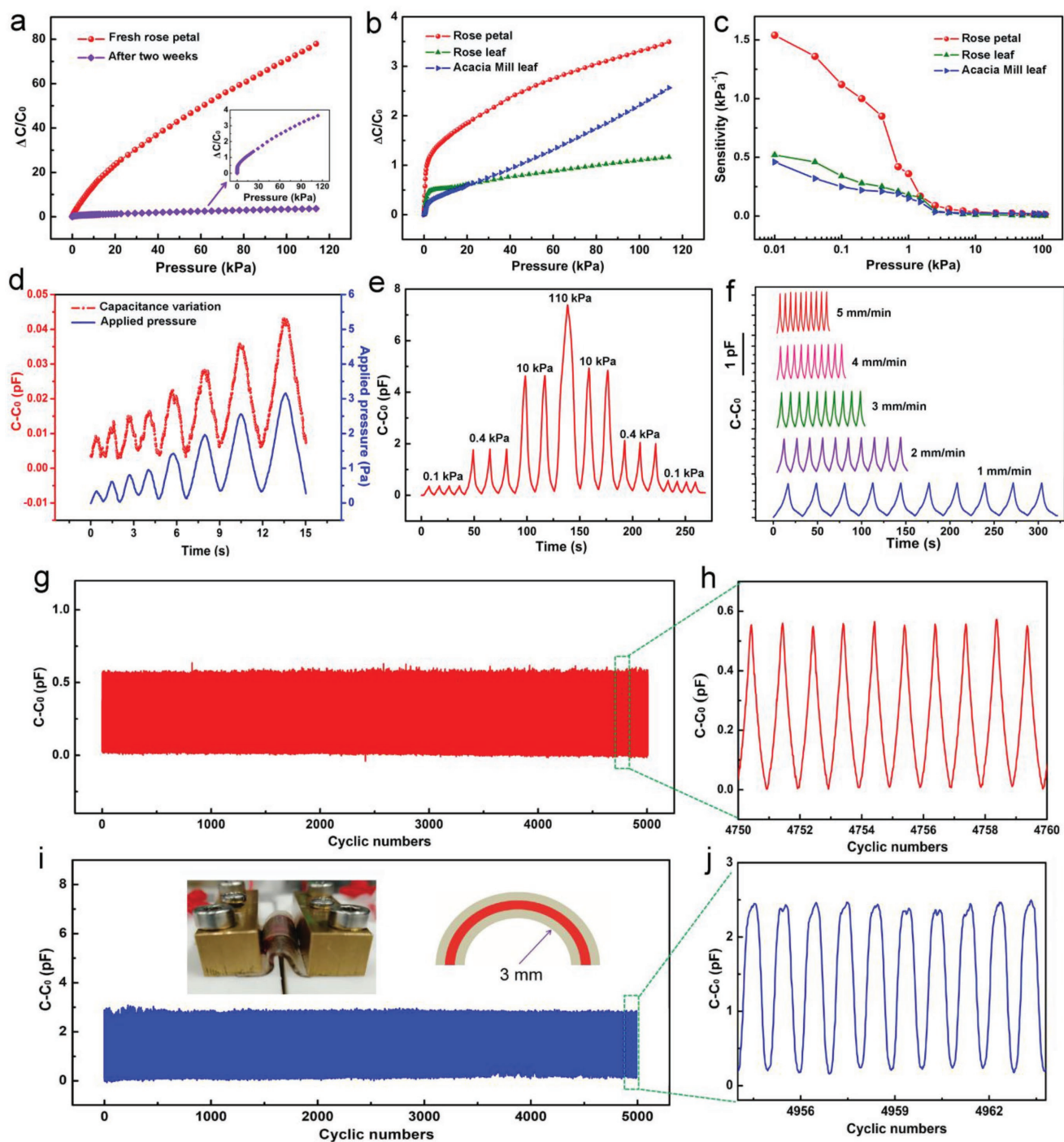


**Figure 2.** Properties of the natural-material-based e-skins. a)  $\Delta C/C_0$  as a function of pressure of the e-skins based on fresh petal and the property after two weeks. b)  $\Delta C/C_0$  as a function of pressure of three types of e-skins based on critical point dried rose petal, rose leaf, and *Acacia Mill* leaf. c) Summary of sensitivities for the natural-materials-based e-skins. d) Time-dependent capacitance variations of the rose petal-based e-skin, showing an LOD at least better than 0.65 Pa. e) Capacitance variations under successive pressures of 0.1, 0.4, 10, and 110 kPa. f) Capacitance variations at a pressure of 200 Pa with different applied speeds from 1 to 5 mm min<sup>-1</sup> with an increment of 1 mm min<sup>-1</sup>. g) Working stability of the e-skin under repeatedly loading/unloading at a pressure of 150 Pa for 5000 cycles. h) Detailed signals from cycle number 4750 to 4760. i) Bending responses over 5000 cyclic tests. j) Magnified signal of ten bending cycles of panel (i), showing that only quite small differences are found for different cycles.

$$C \propto A\epsilon/d$$

(2)

Theoretically, changing the value of either  $A$ ,  $d$ , or  $\epsilon$  would result in capacitance variation. However, in most cases,  $A$  keeps

almost constant upon pressing. For critical point dried rose-petal-based devices, the area  $A$  of the device is  $\approx 1.5$  cm<sup>2</sup>,  $d$  is typically 150–210  $\mu$ m, and corresponding specific capacitance is  $\approx 2.3$  pF·cm<sup>-2</sup>. From Figure 2b, the capacitance increases by

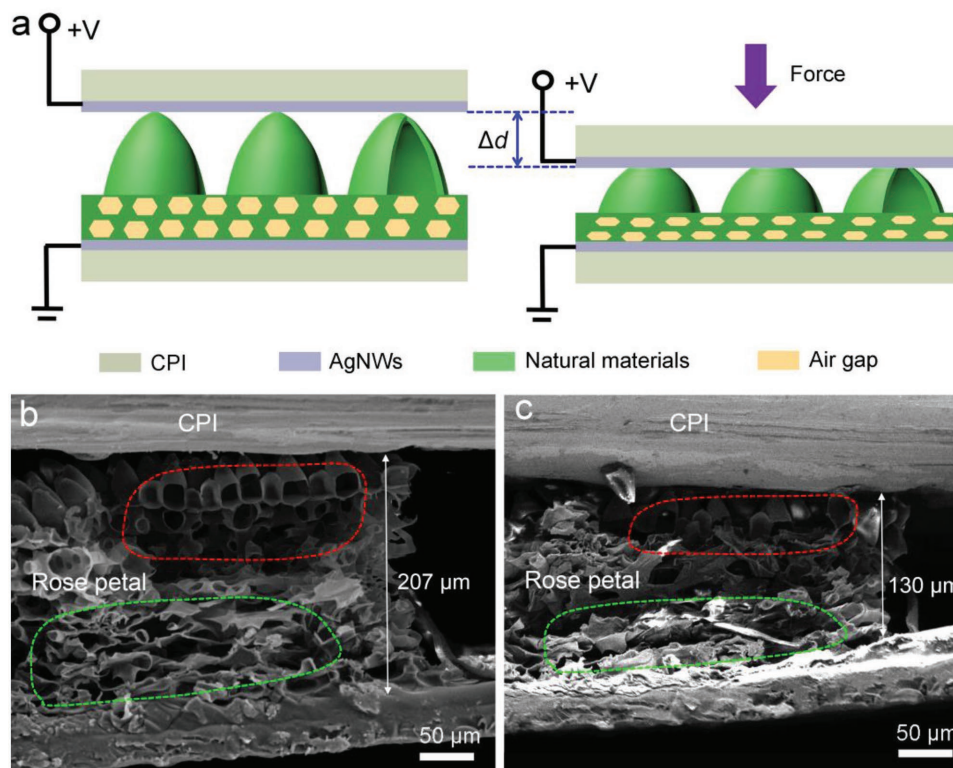


**Figure 3.** The sensing mechanism of the natural-materials-based e-skin. a) Schematic illustration of the e-skin, showing that the hollow structures are compressed upon pressing. b,c) SEM images of a rose petal. The red and green dashed circles indicate the hollow structures b) before and c) after compression, showing that the foam-like structures collapse when applied with pressure.

3.5 times at 115 kPa. Here, the dielectric layer consists of the dried cell walls together with the air gaps filled, as shown in Figure 3a. The compression of the structure is illustrated in Figure 3b,c. Figure 3b is a cross-sectional SEM image of a rose petal in unloading state; it shows foam-like structures, a pattern of dried cell walls and cavities in between. The thickness of the dried cell walls is only  $\approx 700$  nm (Figure S9, Supporting Information), while the cavity size is tens of microns, say, the volume fraction of air gap is far larger than that of the cell walls, and this gives the possibility for the structure to be significantly compressed. Upon loading, the hollow microstructures collapse — the two specific areas indicated by the red and green dotted circles in Figure 3 become significantly thinner, leading to a decrease in dielectric thickness from 207 to 130  $\mu\text{m}$ . Here, unlike the existing works in which the compression of dielectric layer mainly stems from the deformation of surface structures (e.g., PDMS pyramids array,<sup>[20,22]</sup>) the compression of the dried rose petal results from not only the surface structures, but mainly from the compression of the few-layer structures. The function of the hollow architecture can also be confirmed by the fact that a device with naturally dried petal (which does not have a hollow architecture, see Figure S1b, Supporting Information) exhibits a much lower sensitivity, as shown in Figure S10 (Supporting Information). In a naturally dried petal, the mesophyll collapses and leads to a significant decrease in thickness: the critical point dried rose petal is 150–210  $\mu\text{m}$  in thickness, while the naturally dried sample is only  $\approx 60$   $\mu\text{m}$  in thickness, as a result of the collapse of cell walls. The result

is reminiscent of 3D-printed metastructures,<sup>[33]</sup> for which the stiffness can be tuned by geometric design, and such 3D-printed metastructures might be used to design dielectric layer in highly sensitive e-skins if the structures can be printed out at a high resolution and high throughput. In addition to the microstructures, a petal is an intrinsically nonplanar structure, and the macroscale curvature or wrinkles of the dried petal may also contribute to the high sensitivity at low pressures.

On the other hand, the compression increases the permittivity. The change of capacitance ( $C/C_0 = 4.5$  at 115 kPa) is contributed not only by the contraction in thickness  $d$ , but also by the increase in permittivity, which is in return a function of  $d$ . A rough measurement indicates that  $1/d$  increases by  $\approx 3$  times as the pressure increases from 0 to 115 kPa, and this indicates that the permittivity increases by  $\approx 50\%$  at 115 kPa. The effective relative permittivity of the dielectric ( $\epsilon$ ) is given by the equation according to General Lichterecker mixing rule<sup>[34,35]</sup>

$$\epsilon^\alpha = P_{\text{air}} \cdot \epsilon_{\text{air}}^\alpha + P_{\text{cw}} \cdot \epsilon_{\text{cw}}^\alpha \quad (3)$$

where  $\epsilon_{\text{air}}$  and  $\epsilon_{\text{cw}}$  are the permittivity of air and cell walls, respectively;  $P_{\text{air}}$  and  $P_{\text{cw}}$  are the volume fraction of air gap and cell walls, respectively; and  $\alpha$  is a parameter that is determined by the type of mixing rule. Since  $\epsilon_{\text{air}} < \epsilon_{\text{cw}}$  and the volume of the air reduces under loading,  $\epsilon$  will increase as  $d$  decreases.<sup>[34]</sup> The significant change in  $d$  and  $\epsilon$  gives a remarkable capacitance response to external pressure. In general, the compression of the microstructured dielectric layer shows a nonlinear

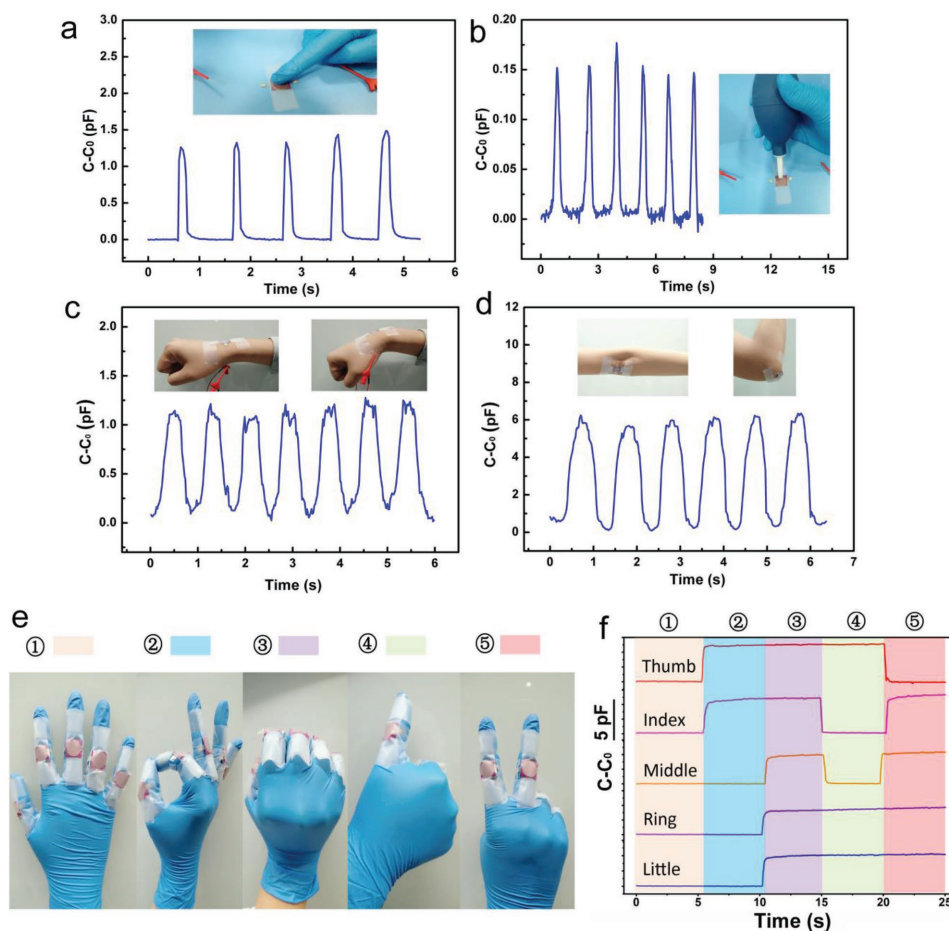


**Figure 4.** Applications of the rose-petal-based e-skin. a) Tactile sensing of the e-skin tested by repeated finger touching. b) Capacitance variations caused by gas flow. c,d) Real-time monitoring of capacitance variations caused by repeated c) wrist bending and d) elbow bending. e) Photographs of the e-skin mounted on five fingers for gesture recognition. f) Capacitive signals at different gestures.

relationship with applied pressure as illustrated in Figure S11 (Supporting Information). The increased deformation can successively activate the mechanoreception under innocuous pressure and a nociception under excess pressure.<sup>[21]</sup> In high pressure regime, the deformation will reach saturation. Therefore, flexible capacitive pressure sensors with microstructured dielectric often show a higher sensitivity under low pressure and the sensitivity decreases with increasing pressure.

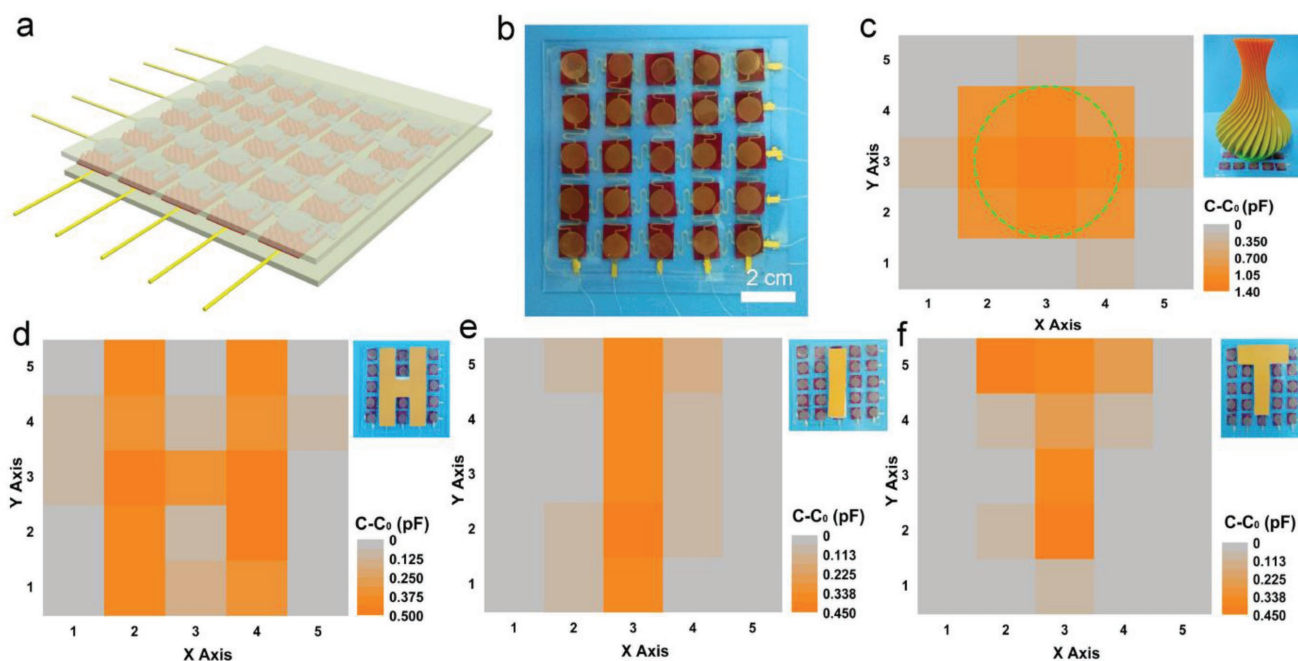
The natural-material-based e-skin has been applied in sensing pressures of different cases, as shown in **Figure 4**. The simple response of the e-skin to normal pressing is exhibited in Figure 4a,b, showing that the skin could respond to repeated finger touching or gas blowing. Here air flow plays the role of a medium that transmits the pressure to the e-skin without direct contact, and the response to air flow may allow for applications in aerodynamics such as pressure detection in a wind tunnel. In addition to sensing of normal pressure, the sensor can also be used to monitor bends generated by wrist (Figure 4c) or elbow (Figure 4d) movement, demonstrating its potential in dynamic human motion inspection.

Figure 4e,f shows a smart glove and its application on gesture recognition. The e-skins were mounted to the five fingers of a plastic glove and connected to an inductance capacitance

and resistance (LCR) meter, as shown in Figure 4e. Each gesture was held for 5 s. At first, five fingers were straightened and the output signals of the five e-skins were in a low initial state. After that, four gestures meaning “OK,” “strong,” “good,” and “yeah” were performed in sequence, and recorded signals well reflect the gestures of the individual fingers as shown in Figure 4f. No delamination or fracture of the devices was observed during the experiment. The ability of gesture recognition is important for artificial intelligence.

The usage of a single flexible tactile sensor is often limited. To test the feasibility of the natural e-skin for tactile sensing, it is desired to build our sensors into a sensor array to spatially map resolved pressure information. **Figure 5a** schematically describes a 5 × 5 pixel array. Totally 25 pieces of dried rose petal were arranged and sandwiched by laser-cut electrodes which were connected by serpentines,<sup>[36]</sup> as shown in Figure 5b. More details for the fabrication of the sensor array can be seen in Experimental Section and Figure S12 (Supporting Information). When loaded with a round-bottom vase onto the sensor array, the mapping of output capacitive signals could well match the touching contour of the vase (Figure 5c). In addition, three PDMS stamps in the shapes of “H,” “I,” and “T” were successively placed on the sensor array. It can be seen that the pixel





**Figure 5.** Pixel array. a) Schematic illustration of e-skin sensors array. Two serpentine-patterned electrodes sandwich 25 pieces of rose petals to form  $5 \times 5$  sensors array. b) Photograph of a  $5 \times 5$  pixel array. c) Pressure distribution mapping of the sensor array when a vase is placed on. The green dotted circle indicates the touching contour of the vase bottom. d–f) Pressure distribution mapping of the sensor array with PDMS stamps in the shapes of “H,” “I,” and “T” on, respectively.

array gives mapped capacitive signals that well match the shape of the PDMS stamps (Figure 5d–f). It should be noted that the capacitance of a pixel can be interfered by the crosstalk of serpentine-like electrodes. However, we found that the crosstalk is a weak effect that can be ignored in many applications: our experiment demonstrated that when the top and bottom electrodes are not aligned (without overlap), the signal is  $\approx 70$  times weaker than the case with fully overlapped electrodes (see Figure S13, Supporting Information). The ability of mapping spatial pressure information is quite similar to the sensing of human skin, and our e-skins offer potential applications in soft robotics and may allow for friendly interaction between a robot and human beings or a robot and the environment.

The natural materials we used in this work are not the sole types that can be used as the dielectric layer for e-skins. It is well known that plant cells have a layer of thin, stiff but elastic cell wall that protects the cytoplasm. In plants, leaves and petals typically consist of a few layers of cells which form a foam-like 3D network; thus the dried leaves or petals play like “microfoam,” an ideal structure as the dielectric layer in e-skins. Such foam-like structures are also found in other parts of a plant from root tips to treetop. In addition, some leaf or petal surfaces have a microstructured rough surface, which is also a favorable design that can significantly improve the sensitivity. Compared with the surface microstructures fabricated by costly microfabrication methods,<sup>[22]</sup> natural materials are environmentally friendly, abundant, easily available, and cost effective. We predict that there will be many other natural materials applied in high performance e-skins.

In summary, we have reported simple and low-cost flexible e-skins that directly use natural materials as the dielectric layer.

Our e-skin shows a high sensitivity of  $1.54 \text{ kPa}^{-1}$ , ultralow LOD as low as 0.6 Pa, the ability of broad-pressure range sensing (0.6 Pa–115 kPa), and high robustness when subjected to at least 5000 cyclic pressings or bends. The e-skin has been applied to monitor human motion, gas flow, as well as sense the spatial pressure distribution, paving the way for the applications in artificial intelligence, soft robotics, wearable electronics, and so forth. We also predict that not only the materials studied here, but many other natural materials of a tremendous of plants might be used in high performance flexible electronic devices.

## Experimental Section

**Preparation of Natural Materials as Dielectrics:** Natural materials were critical point dried by using an automated dryer (Leica EM CPD300, Leica Microsystems GmbH, Germany) after several washing steps in 99.8% ethanol. The drying protocol included slow  $\text{CO}_2$  admittance with a delay of 120 s, six exchange cycles ( $\text{CO}_2$ : 99.8% ethanol), followed by a slow heating (38 °C) process and slow gas discharge. Finally, each sample was cut into  $1.5 \times 1.5 \text{ cm}^2$  as the dielectric layer.

**Preparation of Top and Bottom Electrode, and E-skin:** Colorless polyacetylimide (CPI, thickness: 50  $\mu\text{m}$ ) film was cut into discs with a diameter of 14 mm by using a laser cutter (WE-6040). AgNWs film with a sheet resistance of  $\approx 10 \Omega \cdot \text{sq}^{-1}$  were sprayed on the CPI film by using an air gun (Badger). The synthesis of the AgNWs can be seen in our previous report.<sup>[26]</sup> The adhesion of the AgNWs solution was modified through the addition of polymer HPMC (0.5 wt%). The disc-shaped CPI film coated AgNWs was then dried at 70 °C for 10 min using as the top and bottom electrodes and the natural materials were sandwiched between the electrodes. Finally, the edges were sealed together with 3M Scotch or VHB tape.

*Fabrication of the Pixel Array:* Step 1: CPI discs connected by serpentine were cut by laser cutting to a  $5 \times 5$  array. Step 2: AgNWs were spray coated on the  $5 \times 5$  CPI disc array. Step 3: The laminated film electrodes were connected to silver wires by adhering silver paste and pasted on PDMS. Step 4: The rose petal dielectric layer or other natural dielectrics were settled on the AgNWs/CPI/PDMS electrode. Step 5: Another identical  $5 \times 5$  electrode was placed orthogonally to the rose petal/AgNWs/CPI/PDMS film, face-to-face.

*Characterization and Measurements:* The microstructures of the fresh and the dried rose petals were inspected by field-emission scanning electron microscopy (FE-SEM, TESCAN) operated at 5 kV. The capacitance variations of the e-skin were measured using an LCR meter (E4980AL, KEYSIGHT) with a testing frequency of 1 MHz. A force gauge with a computer-controlled stage (XLD-20E, Jingkong Mechanical testing Co., Ltd) was used to detect the external pressure. The e-skins were fixed on a stage of the testing system for repeatedly loading/unloading tests with different loading speeds and forces. For the bending test, a device was clamped on a home-made flexibility tester and real-time capacitance was recorded. Signed consent was obtained from the volunteer regarding the tests with a volunteer in Figure 4.

## Supporting Information

Supporting Information is available from the Wiley Online Library or from the author.

## Acknowledgements

Y.W. and Z.Q. contributed equally to this work. This work was financially supported by the funds of the “Guangdong Innovative and Entrepreneurial Research Team Program” under contract No. 2016ZT06G587, the National Natural Science Foundation of China (No. 51771089 and U1613204), the “Science Technology and Innovation Committee of Shenzhen Municipality” (Grant No. JCYJ20170817111714314 and JCYJ20160613160524999), and the “Peacock Plan” (No. Y01256120). The authors thank Prof. L. Zhang in the Department of Physics of the Southern University of Science and Technology for the help on critical point dried processes.

## Conflict of Interest

The authors declare no conflict of interest.

## Keywords

electronic skins, flexible pressure sensors, microstructures, natural materials, rose petals

Received: May 1, 2018

Revised: July 2, 2018

Published online: July 29, 2018

- 
- [1] Y. Wan, Y. Wang, C. F. Guo, *Mater. Today Phys.* **2017**, *1*, 61.  
 [2] M. L. Hammock, A. Chortos, B. C. K. Tee, J. B. H. Tok, Z. Bao, *Adv. Mater.* **2013**, *25*, 5997.  
 [3] Y. Zang, F. Zhang, C.-A. Di, D. Zhu, *Mater. Horiz.* **2015**, *2*, 140.  
 [4] T. Someya, Z. Bao, G. G. Malliaras, *Nature* **2016**, *540*, 379.  
 [5] A. Chortos, Z. Bao, *Mater. Today* **2014**, *17*, 321.  
 [6] X. Wang, Z. Liu, T. Zhang, *Small* **2017**, *13*, 1602790.  
 [7] J. Park, Y. Lee, J. Hong, M. Ha, Y. D. Jung, H. Lim, S. Y. Kim, H. Ko, *ACS Nano* **2014**, *8*, 4689.

- [8] M. Jian, K. Xia, Q. Wang, Z. Yin, H. Wang, C. Wang, H. Xie, M. Zhang, Y. Zhang, *Adv. Funct. Mater.* **2017**, *27*, 1606066.  
 [9] Y. Joo, J. Yoon, J. Ha, T. Kim, S. Lee, B. Lee, C. Pang, Y. Hong, *Adv. Electron. Mater.* **2017**, *3*, 1600455.  
 [10] S. C. B. Mannsfeld, B. C. K. Tee, R. M. Stoltenberg, C. V. H. H. Chen, S. Barman, B. V. O. Muir, A. N. Sokolov, C. Reese, Z. Bao, *Nat. Mater.* **2010**, *9*, 859.  
 [11] W. Wu, X. Wen, Z. L. Wang, *Science* **2013**, *340*, 952.  
 [12] D. Y. Park, D. J. Joe, D. H. Kim, H. Park, J. H. Han, C. K. Jeong, J. G. Park, B. Joung, K. J. Lee, *Adv. Mater.* **2017**, *29*, 1702308.  
 [13] R. Liu, X. Kuang, J. Deng, Y.-C. Wang, A. C. Wang, W. Ding, Y.-C. Lai, J. Chen, P. Wang, Z. Lin, H. J. Qi, B. Sun, Z. L. Wang, *Adv. Mater.* **2018**, *30*, 1705195.  
 [14] Z. Lin, J. Chen, X. Li, Z. Zhou, K. Meng, W. Wei, J. Yang, Z. L. Wang, *ACS Nano* **2017**, *11*, 8830.  
 [15] X. D. Wang, L. Dong, H. L. Zhang, R. M. Yu, C. F. Pan, Z. L. Wang, *Adv. Sci.* **2015**, *2*, 1500169.  
 [16] B. Q. Nie, R.Y. Li, J. Cao, J. D. Brandt, T. R. Pan, *Adv. Mater.* **2015**, *27*, 6055.  
 [17] S. Kang, J. Lee, S. Lee, S. Kim, J.-K. Kim, H. Algadi, S. Al-Sayari, D.-E. Kim, D. Kim, T. Lee, *Adv. Electron. Mater.* **2016**, *2*, 1600356.  
 [18] S. Chen, B. Zhuo, X. Guo, *ACS Appl. Mater. Interfaces* **2016**, *8*, 20364.  
 [19] D. Kwon, T.-I. Lee, J. Shim, S. Ryu, M. S. Kim, S. Kim, T.-S. Kim, I. Park, *ACS Appl. Mater. Interfaces* **2016**, *8*, 16922.  
 [20] B. C. K. Tee, A. Chortos, R. R. Dunn, G. Schwartz, E. Eason, Z. Bao, *Adv. Funct. Mater.* **2014**, *24*, 5427.  
 [21] Y. L. Zhang, Y. S. Fang, J. Li, Q. H. Zhou, Y. J. Xiao, K. Zhang, B. B. Luo, J. Zhou, B. Hu, *ACS Appl. Mater. Interfaces* **2017**, *9*, 37493.  
 [22] G. Schwartz, B. C. K. Tee, J. G. Mei, A. L. Appleton, D. H. Kim, H. L. Wang, Z. Bao, *Nat. Commun.* **2013**, *4*, 1859.  
 [23] T. Li, H. Luo, L. Qin, X. Wang, Z. Xiong, H. Ding, Y. Gu, Z. Liu, T. Zhang, *Small* **2016**, *12*, 5042.  
 [24] H. Kim, G. Kim, T. Kim, S. Lee, D. Kang, M. S. Hwang, Y. Chae, S. Kang, H. Lee, H. G. Park, W. Shim, *Small* **2018**, *14*, 1703432.  
 [25] Y. Joo, J. Byun, N. Seong, J. Ha, H. Kim, S. Kim, T. Kim, H. Im, D. Kim, Y. Hong, *Nanoscale* **2015**, *7*, 6208.  
 [26] Y. Wan, Z. Qiu, Y. Hong, Y. Wang, J. Zhang, Q. Liu, Z. Wu, C. F. Guo, *Adv. Electron. Mater.* **2018**, *4*, 1700586.  
 [27] R. Y. Li, Y. Si, Z. J. Zhu, Y. J. Guo, Y. J. Zhang, N. Pan, G. Sun, T. R. Pan, *Adv. Mater.* **2017**, *29*, 1700253.  
 [28] Z. X. Tang, L. E. Scriven, H. T. Davis, *J. Chem. Phys.* **1992**, *97*, 494.  
 [29] Z. Qiu, Y. Wan, W. Zhou, J. Yang, J. Yang, J. Huang, J. Zhang, Q. Liu, S. Huang, N. Bai, Z. Wu, W. Hong, H. Wang, C. F. Guo, *Adv. Funct. Mater.* **2018**, <https://doi.org/10.1002/adfm.201802343>.  
 [30] Y. Pang, K. Zhang, Z. Yang, S. Jiang, Z. Ju, Y. Li, X. Wang, D. Wang, M. Jian, Y. Zhang, R. Liang, H. Tian, Y. Yang, T.-L. Ren, *ACS Nano* **2018**, *12*, 2346.  
 [31] W. Zhong, Q. Liu, Y. Wu, Y. Wang, X. Qing, M. Li, K. Liu, W. Wang, D. Wang, *Nanoscale* **2016**, *8*, 12105.  
 [32] J. Lee, H. Kwon, J. Seo, S. Shin, J. H. Koo, C. Pang, S. Son, J. H. Kim, Y. H. Jang, D. E. Kim, T. Lee, *Adv. Mater.* **2015**, *27*, 2433.  
 [33] X. Y. Zheng, H. Lee, T. H. Weisgraber, M. Shusteff, J. DeOtte, E. B. Duoss, J. D. Kuntz, M. M. Biener, Q. Ge, J. A. Jackson, S. O. Kucheyev, N. X. Fang, C. M. Spadaccini, *Science* **2014**, *344*, 1373.  
 [34] Y. G. Wu, X. H. Zhao, F. Li, Z. G. Fan, *J. Electroceram.* **2003**, *11*, 227.  
 [35] K. Lichtennecker, *Phys. Z.* **1926**, *27*, 115.  
 [36] J. Kim, M. Lee, H. J. Shim, R. Ghaffari, H. R. Cho, D. Son, Y. H. Jung, M. Soh, C. Choi, S. Jung, K. Chu, D. Jeon, S.-T. Lee, J. H. Kim, S. H. Choi, T. Hyeon, D.-H. Kim, *Nat. Commun.* **2014**, *5*, 5747.